Start-of-run versus end-of-run kinetics for COS and CS_2 conversion across Claus catalysts

Christopher B. Lavery, Dao Li, Ruohong Sui, and Robert A. Marriott

Alberta Sulphur Research Ltd.
Contacts: rob.marriot@ucalgary.ca and cblavery@ucalgary.ca

Abstract

The conversion of CS_2 and COS across the catalyst beds within a modified Claus sulfur recovery unit typically operates in the chemically limited kinetic regime. As such, the temperature-dependent rate constants for the hydrolysis of CS_2 and COS across Claus Al_2O_3 or TiO_2 catalysts can be valuable tools for design and optimisation. In this context, ASRL has previously reported the activation energies (E_a) and pre-exponential factors (A) for CS_2 and COS destruction across Claus Al_2O_3 and TiO_2 at start-of-run conditions. More recently, we have expanded this research to include several commercially available Al_2O_3 and TiO_2 materials that have been hydrothermally aged in our laboratories to simulate end-of-run conditions. Our methodology and end-of-run results will be described herein and compared against the previously published start-of-run data.

Introduction

Sulfuric acid (H_2SO_4) is the most abundantly manufactured chemical in the world (*ca*. 260 million tons per annum).[1] The primary sulfur feedstock for production of H_2SO_4 is from the modified Claus process (*ca.* 70 million tons per annum).[2] Indeed, the modified Claus process is an equilibrium limited system whereby H_2S is converted to elemental sulfur and H_2O across a thermal reactor and several catalysts beds operated at successively lower temperatures (Figure 1). A theoretical sulfur recovery of 98% is possible with three catalyst beds; however, sulfur recovery efficiencies of up to >99.9% can be obtained if implemented in combination with the appropriate tail gas cleanup (TGCU) technology. However, such high recoveries require both the thermal and catalytic stages to operate at optimal efficiency. This is complicated by acid gas contamination with impurities such as hydrocarbons (gas plant scenario) and / or ammonia (refinery scenario). Furthermore, the amount of hydrocarbon contamination has a marked influence on concentrations of both CS_2 and COS that form within thermal reactor and end up reaching the Claus catalyst beds.[3] At thermal reactor temperatures, CS_2 can be formed from direct reaction between hydrocarbons and elemental sulfur as shown in reaction 1. While most COS arises from recombination of CO and sulfur upon cooling of these species in the waste heat boiler (reaction 2), there are a multitude of other interlinked transformations at play that will influence this overall reaction which may also lead to COS formation.[3] See reference 3 for a detailed discussion on reactions involving COS in the thermal reactor.

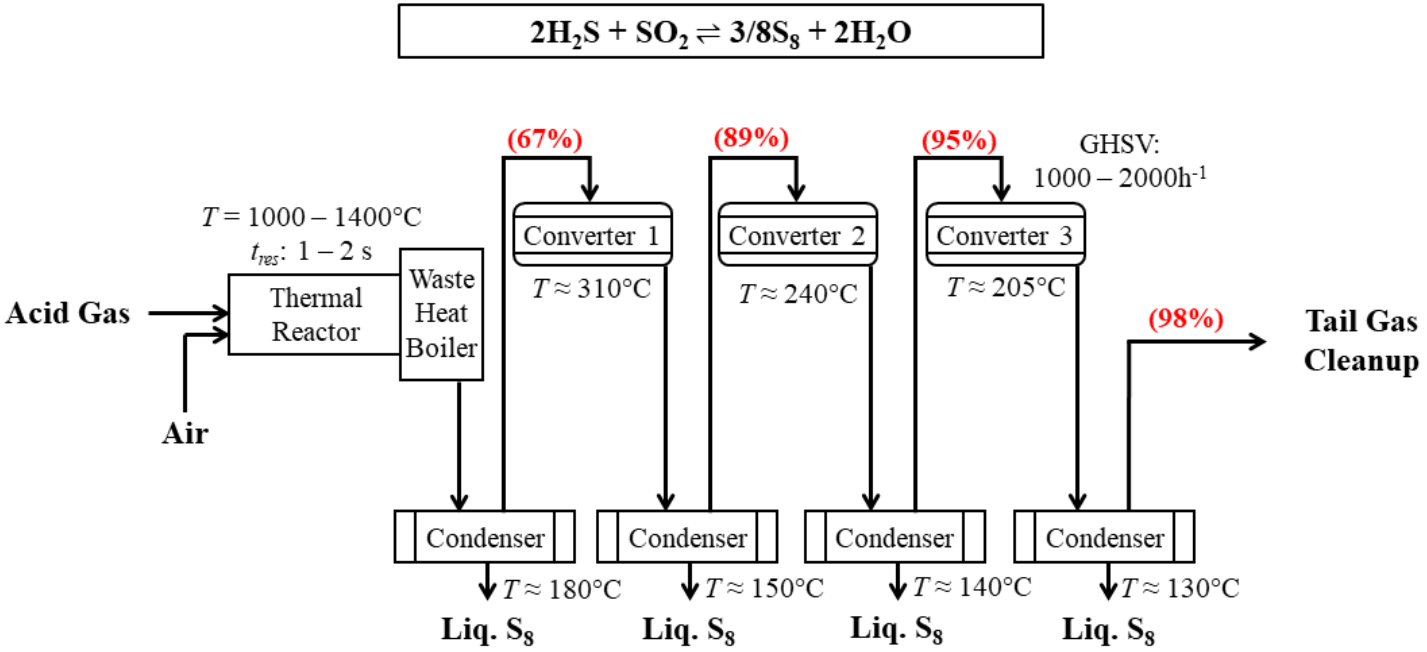

Figure 1. Simplified schematic of the modified Claus process with corresponding sulfur recoveries after each stage in red.

$$CH_4 + 2S_2 \rightarrow CS_2 + 2H_2S \quad \text{(reaction 1)}$$

$$2CO + S_2 \rightarrow 2COS \quad \text{(reaction 2)}$$

Although some destruction occurs in the thermal reactor, any extraneous CS_2 and COS that persist through the thermal reactor and waste heat boiler must be destroyed across the catalytic converters according to reactions 3 and 4, respectively.

$$CS_2 + 2H_2O \rightarrow 2H_2S + CO_2 \quad \text{(reaction 3)}$$

$$COS + H_2O \rightarrow H_2S + CO_2 \quad \text{(reaction 4)}$$

Equilibrium allows for quantitative CS_2 destruction and very high COS (>99%) conversions. However, reactions 3 and 4 typically operate in the kinetic regime, *i.e.*, below equilibrium conversion, under industrial Claus conditions. Therefore, the temperature dependent rate constants for the hydrolysis of CS_2 and COS across Claus Al_2O_3 and TiO_2 catalysts are valuable tools for the design and optimising of new, as well as existing, sulfur recovery units. Indeed, in some cases, up to 50% of sulfur recovery losses can be attributed to inefficient CS_2 and COS destruction.[4]

Previous studies on the kinetics of COS and CS_2 hydrolysis on both Al_2O_3 and TiO_2 catalysts were not performed with a full Claus feed.[5,6] This is particularly relevant, because when an Al_2O_3 or TiO_2 catalyst is exposed to Claus conditions, a steady state surface loading of sulfate, thiosulfate and water species will be realized. ASRL has shown that the adsorbed sulfate has a direct impact on the rate of CS_2 and COS hydrolysis.[7] Furthermore, the H_2S / SO_2 ratio is the primary factor that dictates the steady state concentration of these sulfate species under normal operating conditions.[8] Therefore, if laboratory determined kinetic data for CS_2 and COS conversion is going to be applied to a field scenario, it is crucial that the data be collected under representative conditions. In this context, we have measured CS_2 and COS hydrolysis rate constants over a range of temperatures for both Al_2O_3 and TiO_2 catalysts under start-of-run[9] and, more recently, end-of-run first converter conditions. We will report herein on our methodology, the utility of the kinetic parameters calculated from our data, and draw comparisons between our start-of-run and end-of-run results.

Materials and Methods

For safety reasons, the laboratory equipment discussed below is housed within a ballistic ventilated walk-in bay containing H_2S and SO_2 detectors which shut off air operated supply gas valves when in high-alarm (≥10 ppm).

All experiments were executed in a vertical stainless steel fixed-bed reactor with a 2.5 cm o.d. × 39.4 cm length and an i.d. of 2.1 cm that has been described previously and is shown schematically in Figure 2.[10] In short, the reactor temperature was controlled isothermally (± 1°C) over its full length by means of an air-ebulliated sand bath. Isothermal control was confirmed by a series of 6 axially located thermocouples (not shown in the schematic). The majority of the gases were delivered to the reactor by use of Bruker mass flow controllers; however, H_2O was introduced *via* a Waters HPLC pump. Any elemental sulfur formed during experimental runs was removed by

condensation with in-line sulfur traps ($T \approx 50$°C). All gases were purchased from Praxair Canada and had purities greater than 99.9%.

For each of the experiments, the stainless-steel reactor was charged with either 25 mL of Claus Al_2O_3 or TiO_2 catalyst. A suite of experiments consisted of measuring CS_2 and COS hydrolysis at 330, 300 and 260°C, with total flow rates corresponding to gas hourly space velocities (GHSVs) of 5000, 2400, 1440 and 1000 h^{-1} (T_{ref} = 25°Cand p_{ref} = 1 atm). These GHSVs corresponded to actual catalyst contact times of i) 0.35, 0.73, 1.25 and 1.75 s at 330°C; ii) 0.36, 0.77, 1.31 and 1.84 s at 300°C; and iii) 0.40, 0.82, 1.41 and 1.98 s at 260°C. The composition of the representative first converter feed employed was 58.1 % N_2, 7.9 % H_2S, 4.0 % SO_2, 30 % H_2O and either 0.1% CS_2 or 0.1 % COS. By measuring CS_2 and COS conversion under each set of experimental conditions described above, the corresponding pseudo-first order plots were prepared. Using CS_2 as an example, the derivation of the integrated pseudo-first order equation, used for plotting our experimental conversions, is shown below and has been described previously.[11]

The rate of CS_2 hydrolysis across a Claus catalyst under representative first converter conditions can be described as

$$-\frac{[CS_2]}{dt} = k[CS_2]^a \, f(H_2O)[Q]^b . \qquad \text{(equation 1)}$$

While $f(H_2O)$ is a function of the concentration of H_2O in the feed, the catalyst surface concentration of H_2O will be in such large excess that it can be considered constant across our experiments. Additionally, $[Q]$ represents the surface density of catalyst active sites and can also be considered constant if the same catalysts are employed across the different temperature and GHSV pairings. Therefore, $f(H_2O)$ and $[Q]^b$ can be incorporated into the pseudo rate constant k' and equation 1 can be rewritten as

$$-\frac{[CS_2]}{dt} = k'[CS_2]^a . \qquad \text{(equation 2)}$$

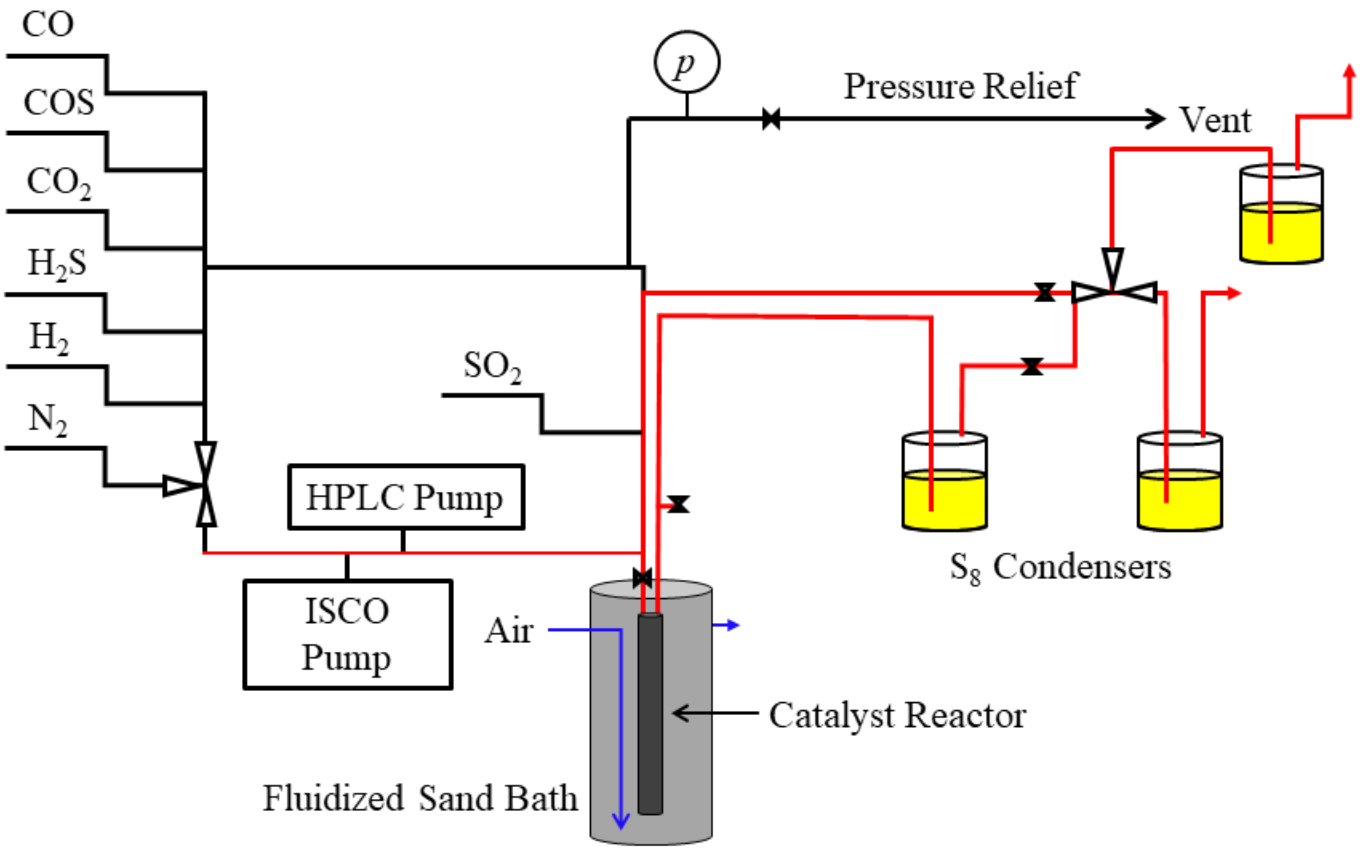

Figure 2. Simplified schematic of the ebulliated sand bath catalyst reactor.

If a = 1 and the initial concentration of CS_2 is described as $[CS_2]^\circ$, then the integrated form rate equation is

$$[CS_2] = [CS_2]^\circ e^{-k't}, \qquad \text{(equation 3)}$$

which can also be written as

$$CS_2 \text{ conversion} = \frac{[CS_2]^\circ - [CS_2]}{[CS_2]^\circ} = 1 - e^{-k't}. \qquad \text{(equation 4)}$$

The linear form of the pseudo-first order rate equation is then obtained by rearranging and taking the natural logarithm of each side

$$\ln\left(1 - CS_2 \text{ conversion}\right) = -k't, \qquad \text{(equation 5)}$$

Where the term t represents catalyst contact time in seconds and can be determined from the GHSV and temperature of the test. The methodology described above allowed us to determine the pseudo first order rate constant for each experimental temperature (330, 300 and 260°C). However, to allow for a rate constant to be determined at any temperature within our experimental range, we used these k' values to fit the corresponding Arrhenius equation:

$$k' = Ae^{-E_a/RT}, \qquad \text{(equation 6)}$$

where E_a represents the activation energy, A is an empirical frequency factor or pre-exponential factor, R is the gas constant, and T is temperature.

Prior to performing any experiments, the fresh Al_2O_3 or TiO_2 was pre-sulfated at 320 °C by flowing a feed consisting of 58.0 % N_2, 8.0 % H_2S, 4.0 % SO_2, and 30.0 % H_2O for eight hours (GHSV = 1000 h^{-1}). In our start-of-run experiments, this was followed by a sixteen-hour hydrothermal ageing process at the same temperature and GHSV but with a feed containing 71.5 % N_2, 9.5 % CO_2 and 19 % H_2O. To simulate end-of-run conditions, the hydrothermal ageing temperature was increased to 500°C. On average, this higher temperature resulted in a *ca.* 50% surface area reduction compared to the fresh material (Figure 3).

Any initial oxygen in the bed was removed by flushing with high-purity N_2 and the catalyst was maintained under a small flow of N_2 (*ca.* 50 mL·min^{-1}) during all overnight and weekend periods. Bringing the different feed streams into and out of the catalyst bed was performed by diverting the stream to bypass, initiating H_2S, SO_2, H_2O and either CS_2 or COS flow, and then redirecting the stream back through the reactor. This procedure was adopted to ensure the catalyst bed was either exposed to just N_2 or the full challenge feed. For each suite of experiments, the time on stream for the test performed at T = 330°C / GHSV = 5000 h^{-1} was eight hours. In all cases CS_2 and COS hydrolysis had appeared to stabilize after four hours under these conditions. Therefore, four hours was considered sufficient to obtain stabilized conversions in the remaining tests.

Using CS_2 as an example, conversions were calculated according to equation 7,

$$\%\,\mathrm{CS_2}\ \text{conversion} = 100\left(1 - \frac{x_{prod}(\mathrm{CS_2})x_{feed}(\mathrm{N_2})}{x_{feed}(\mathrm{CS_2})x_{prod}(\mathrm{N_2})}\right), \qquad \text{(equation 7)}$$

where x_{feed} and $x_{prod.}$ are the mole fractions in the feed and product streams respectively. This approach uses the inert N_2 as an internal standard, to correct for molar changes in the product stream due to either reaction or intentional removal of condensable products (sulfur and H_2O).

Analysis of the product stream for N_2, H_2S, SO_2, COS, and CS_2 was performed on a Varian 3800 gas chromatograph (GC) equipped with parallel Restek Mol-sieve 5Å and U-Bond columns and thermal conductivity detectors (TCDs). Analysis of CO_2 was measured on an SRI 8610 GC equipped with Restek U-Bond and Mol-sieve 5Å columns and two TCDs. These analyses were obtained on a dry and sulfur-free basis by sampling through a cartridge packed with P_2O_5, *i.e.*, water removal quenches the potential of further Claus reaction on GC stationary phase or any condensable water phase. Again, N_2 was used as an internal standard to determine gaseous concentrations as shown in equation 7 and elemental sulfur was calculated based on mass balance.

During each run, duplicate analyses of the product stream were obtained every hour. For reference, the experimental results were compared to equilibrium results calculated using an in-house Gibbs Free Energy minimization program containing thermodynamic data from the most recent JANAF tables. In all scenarios, our experimental Claus conversions were in good agreement with the analogous calculated results.

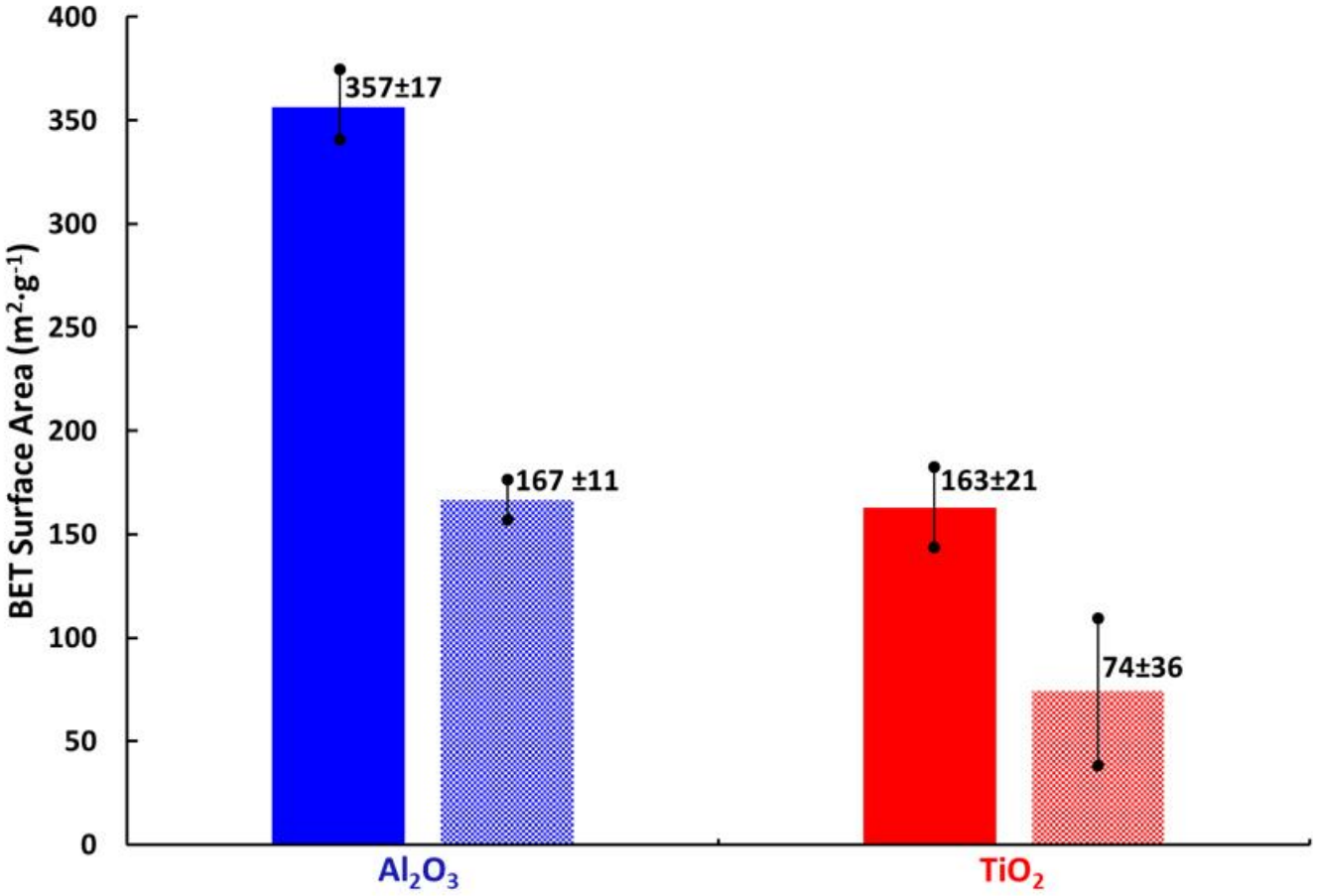

Figure 3. Surface area reduction upon end-of run conditioning (solid bars represent average surface area of fresh materials).

Results and Discussion

A comparison of our previously acquired CS_2 and COS conversion data, under start-of-run conditions, to our more recently obtained end-of-run data is presented across Table 1 and Figures 4-6. While only one Al_2O_3 and one TiO_2 material were assessed in our start-of-run experiments, several different commercially available samples of each were tested in our end-of-run studies. As such, the end-of-run conversions displayed in Figures 4-6 are an average of the performances, with the associated standard deviation (shown by the error bars), offered by the full range materials. As can be seen, in all instances TiO_2 provided superior performance compared to Al_2O_3 and, under analogous conditions, COS conversion levels were higher than those for CS_2. As expected, conversion levels for both CS_2 and COS decreased with increasing GHSV and decreasing temperature. This is typical behaviour for reactions operating in a chemically limited regime. In some instances, particularly for COS conversion across Al_2O_3, the average end-of-run of conversions were higher than the corresponding start-of-run conversions. This is simply because some of the new catalysts included in our end-of-run studies offered better conversions than the one material that was selected for use in our initial start-of-run tests. However, if each individual material were tested under start-of-run conditions, the conversions would be higher than the corresponding end-of-run conversions. The differences in performances between the various commercial materials that were tested was most noticeable under the more stringent test conditions (*i.e.*, in the high GHSV and low temperature experiments).

With the above data in hand, we first prepared the pseudo-first order plots for CS_2 and COS conversion over Al_2O_3 (Figures 7 and 9) and then used the least square fit rate constants to fit the corresponding Arrhenius plots (Figures 8 and 10). Where our start-of-run data has been reported previously,[9] only the end-of-run plots will be presented here. However, the start-of-run rate constants and kinetic parameters will be included here for the sake of comparison and convenience to the reader. As can be seen from the kinetic data presented in Table 2 for Al_2O_3, the conversion of CS_2 was impacted more by the end-of-run conditioning than the reaction of COS. For CS_2 there was in fact a small decrease in activation energy from 57.0±3.7 to 44.3±1.4 $kJ \cdot mol^{-1}$; however, the lower CS_2 conversions in our end-of-run tests is captured by the smaller pre-exponential factor; 64861 versus 4024 s^{-1}. Interestingly, our end-of-run activation energy for CS_2 conversion across alumina is actually in better agreement with the only other value available in the open literature of 40.4 $kJ \cdot mol^{-1}$.[6] As alluded to above, owing to the broader selection of catalysts included in our end-of-run experiments, the corresponding COS end-of-run rate constants were modestly higher than in the analogous start-of-run tests. However, upon completing the full kinetic workup, the activation energies (33.4±0.4 versus 36.3±0.5 $kJ \cdot mol^{-1}$) and pre-exponential factors (1342 versus 3058 s^{-1}) were quite similar. For reference, an activation energy of 25.3 $kJ \cdot mol^{-1}$ has been reported for COS conversion across Al_2O_3 where the only feed components were COS and H_2O.[5]

Table 1. Comparison of start-of-run versus end-of-run conversions.

	Al_2O_3				TiO_2			
	Start-of-run CS_2	**End-of-run CS_2**	**Start-of-run COS**	**End-of-run COS**	**Start-of-run CS_2**	**End-of-run CS_2**	**Start-of-run COS**	**End-of-run COS**
330°C								
5000 h^{-1}	34.7	28.4±2.9	66.0	64.5±14.6	76.8	62.9±22.1	93.8	84.4±9.8
2400 h^{-1}	52.6	42.7±7.3	88.0	87.7±4.8	91.7	79.7±16.1	98.9	95.6±5.6
1440 h^{-1}	67.7	61.1±2.8	94.8	95.4±3.1	97.5	89.1±11.9	99.4	98.8±1.7
1000 h^{-1}	76.6	70.3±4.9	97.2	97.7±2.0	99.3	94.0±8.0	99.5	99.6±0.4
300°C								
5000 h^{-1}	28.6	17.1±3.2	52.1	55.6±17.2	60.5	47.5±31.6	85.1	78.0±12.5
2400 h^{-1}	40.2	29.0±5.7	74.7	80.2±8.4	79.4	61.2±29.5	95.6	90.3±8.9
1440 h^{-1}	54.9	44.9±3.6	85.7	91.0±6.8	89.8	73.5±23.7	98.1	96.8±3.2
1000 h^{-1}	62.3	53.1±3.6	92.4	95.7±4.1	95.5	83.2±19.9	99.2	98.8±1.3
260°C								
5000 h^{-1}	13.3	8.5±5.9	29.0	43.4±19.7	43.1	21.5±10.2	68.9	60.7±15.1
2400 h^{-1}	20.8	17.3±5.7	49.2	63.6±17.1	54.4	33.5±9.6	88.2	78.3±14.2
1440 h^{-1}	30.8	25.1±4.4	64.7	76.5±14.5	64.5	47.5±13.3	95.6	90.0±7.8
1000 h^{-1}	32.6	33.3±5.5	78.0	85.5±10.6	72.9	58.9±12.9	97.4	94.8±4.4

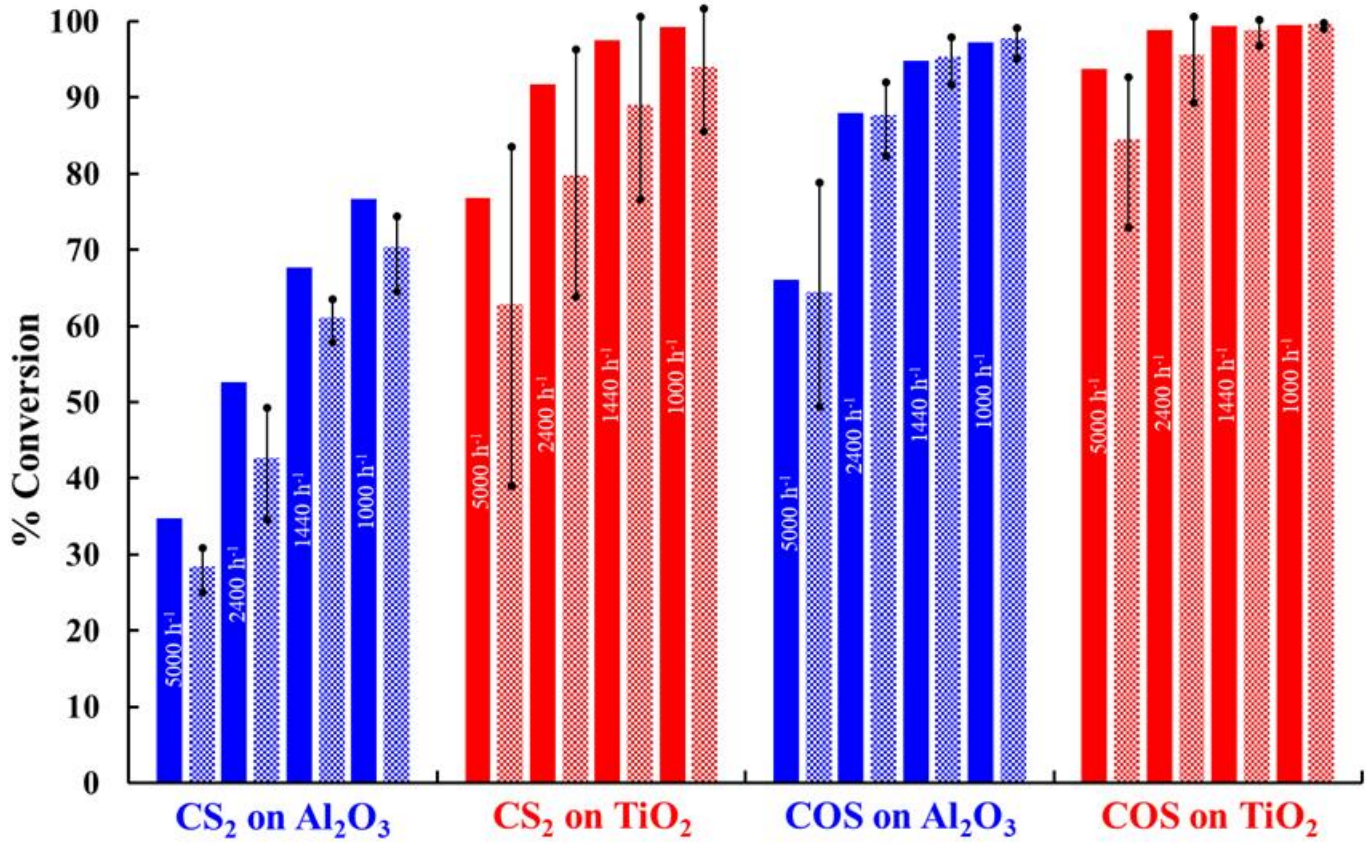

Figure 4. Start-of-run (solid bars) versus end-of-run (checkered bars) conversions at 330°C. Error bars show the standard deviation of results from multiple catalysts.

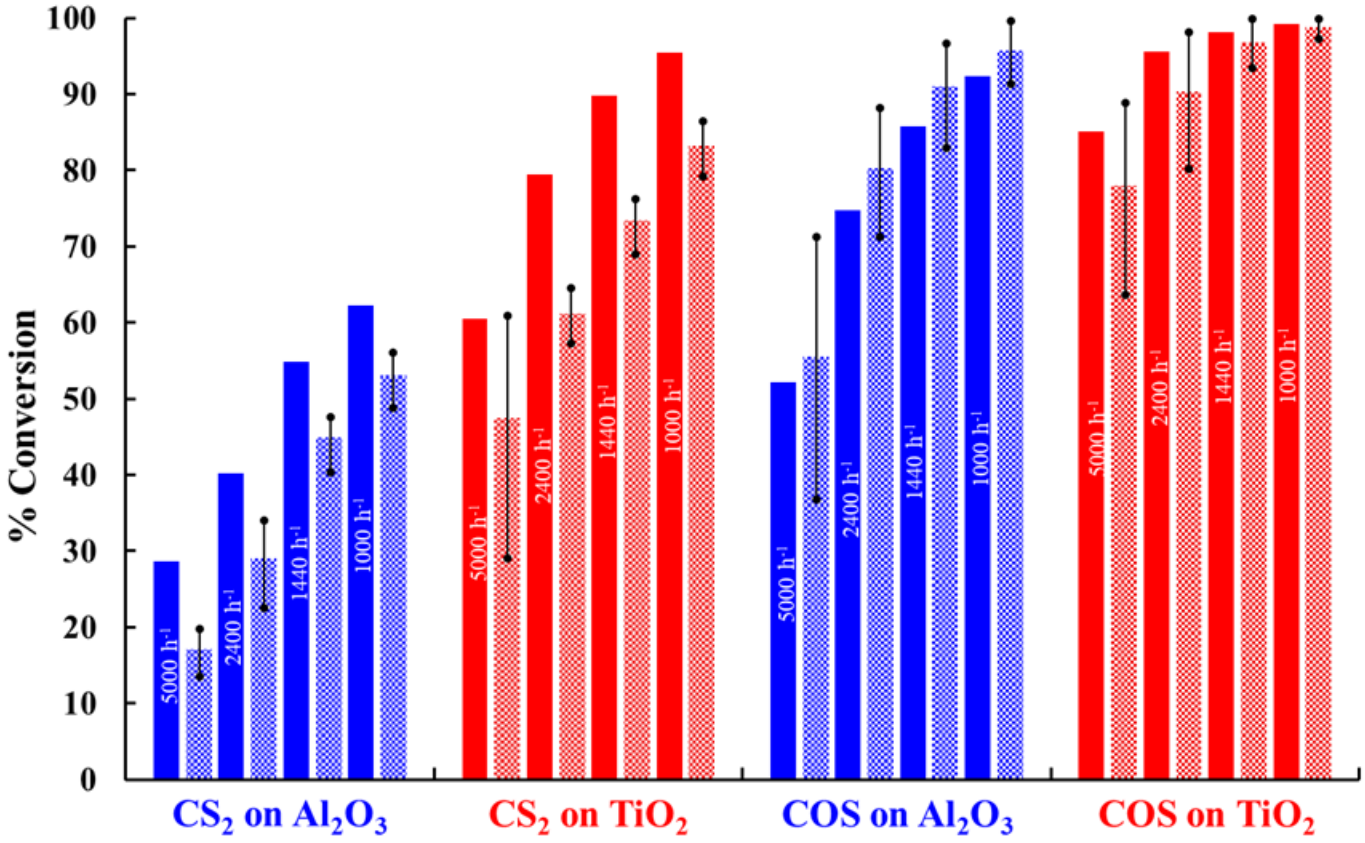

Figure 5. Start-of-run (solid bars) versus end-of-run (checkered bars) conversions at 300°C. Error bars show the standard deviation of results from multiple catalysts.

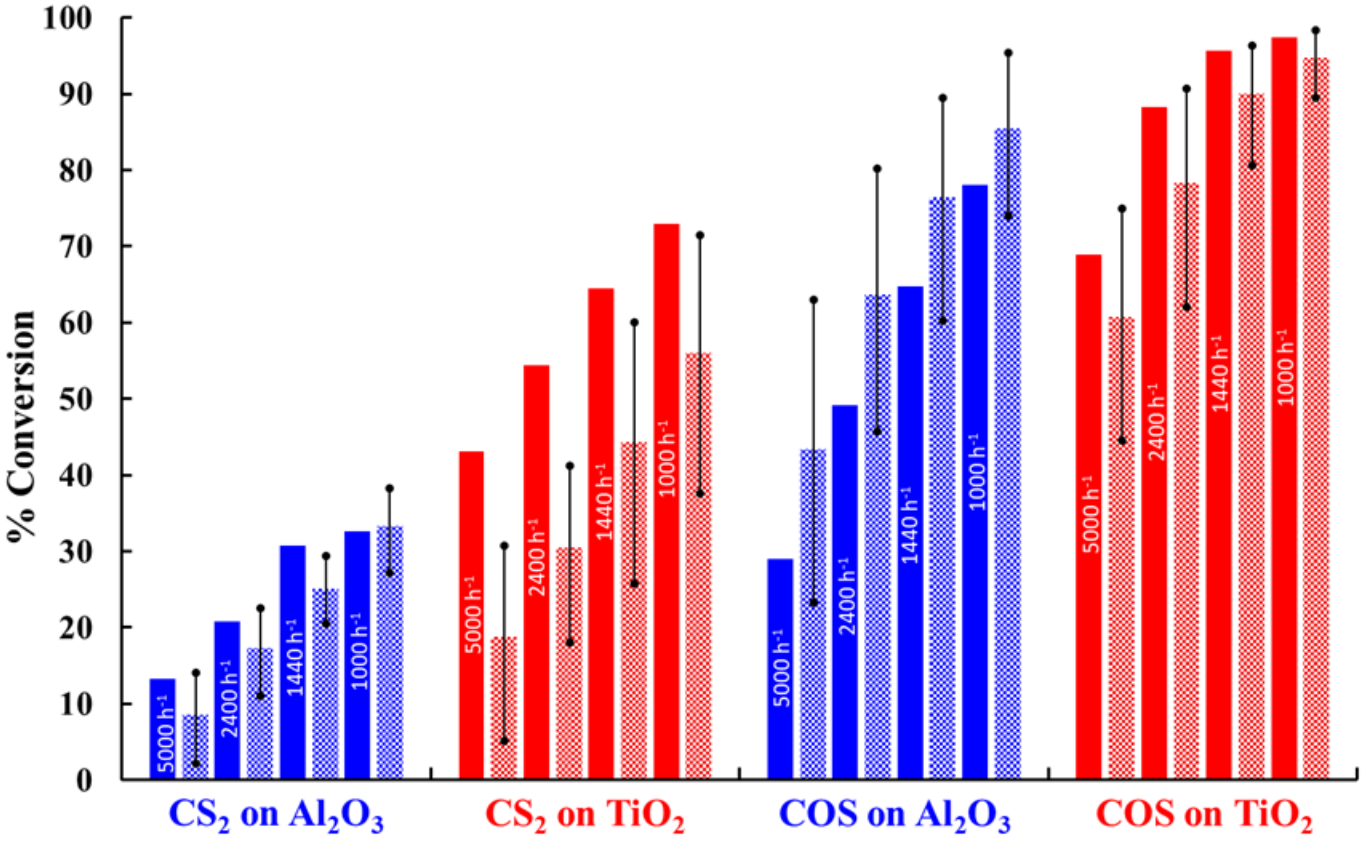

Figure 6. Start-of-run (solid bars) versus end-of-run (checkered bars) conversions at 260°C. Error bars show the standard deviation of results from multiple catalysts.

Table 2. Comparison of empirically determined Al_2O_3 rate constants and kinetic parameters under start-of-run versus end-of-run conditions.

	Al_2O_3			
	Start-of-run CS_2	**End-of-run CS_2**	**Start-of-run COS**	**End-of-run COS**
260°C / k'	0.17±0.03	0.20±0.01	0.73±0.03	0.84±0.09
300°C / k'	0.44±0.03	0.39±0.02	1.22±0.06	1.56±0.09
330°C / k'	0.73±0.03	0.64±0.03	1.75±0.22	2.16±0.09
E_a (kJ·mol^{-1})	**57.0±3.7**	**44.2±1.4**	**33.4±0.4**	**36.3±0.5**
A (s^{-1})	**64861**	**4024**	**1342**	**3058**

In the same format as above, the pseudo-first order plots for CS_2 and COS conversion over TiO_2 are presented in Figures 11 and 13, and the matching Arrhenius plots are provided in Figures 12 and 14. Similarly, the TiO_2 start-of-run rate constants and kinetic parameters are presented in Table 3 for comparison against the analogous end-of-run values. As was observed for CS_2 over Al_2O_3, the end-of-run activation energy activity for CS_2 conversion across TiO_2 (45.1±2.0 kJ·mol^{-1}) was determined to be lower compared to the analogous start-of-run value (64.6±5.8 kJ·mol^{-1}). While experimental error cannot be ruled out, a significant change in activation energy may be indicative of a different conversion mechanism becoming more prevalent. Indeed, in addition to the hydrolysis reaction, CS_2 and COS reaction with SO_2, according to reactions 5 and 6, has been shown to be a plausible pathway for conversion across TiO_2 under Claus conditions.[12] However, more studies are necessary to probe if these reactions contribute significantly to overall conversions.

$$CS_2 + SO_2 \rightarrow 3/2S_2 + CO_2 \qquad \text{(reaction 5)}$$

$$2COS + SO_2 \rightarrow 3/2S_2 + 2CO_2 \qquad \text{(reaction 6)}$$

The conversion of COS across TiO_2 was approaching equilibrium in our previous start-of-run experiments, with measurements at T = 330°C / GHSV = 1000 h^{-1} (contact time = 1.75 s) reaching >99.5%. This approach to equilibrium caused a decreased sensitivity in temperature dependence. As such, all three start-of-run rate constants for this reaction that are presented in Table 3 are in statistical agreement, despite the different temperatures. To find a statistically significant activation energy under start-of-run conditions would require lowering the temperature below the dew point or increasing the GHSV beyond what is practical for our system. However, under end-of-run conditions, the conversions were far enough removed from equilibrium that we did observe a statistical difference in our rate constants, thereby allowing us to define an activation energy of 25.7±0.2 kJ·mol^{-1} and pre-exponential factor of 433 s^{-1}. For comparison, an activation energy of 41.8 kJ·mol^{-1} has been reported COS hydrolysis on TiO_2.[5]

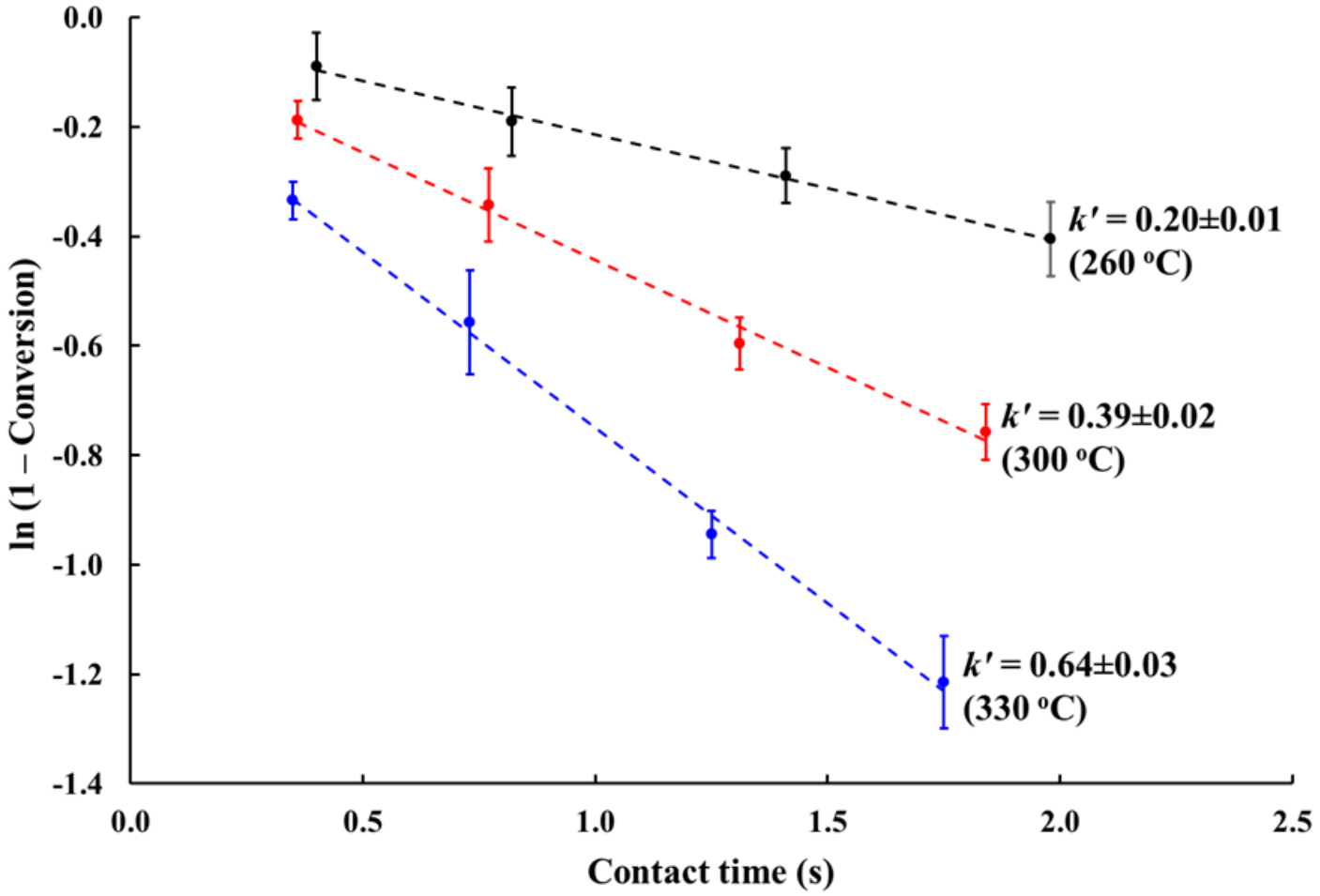

Figure 7. Pseudo-first order plots for CS_2 conversion across Al_2O_3 under end-of-run conditions using pooled conversion data.

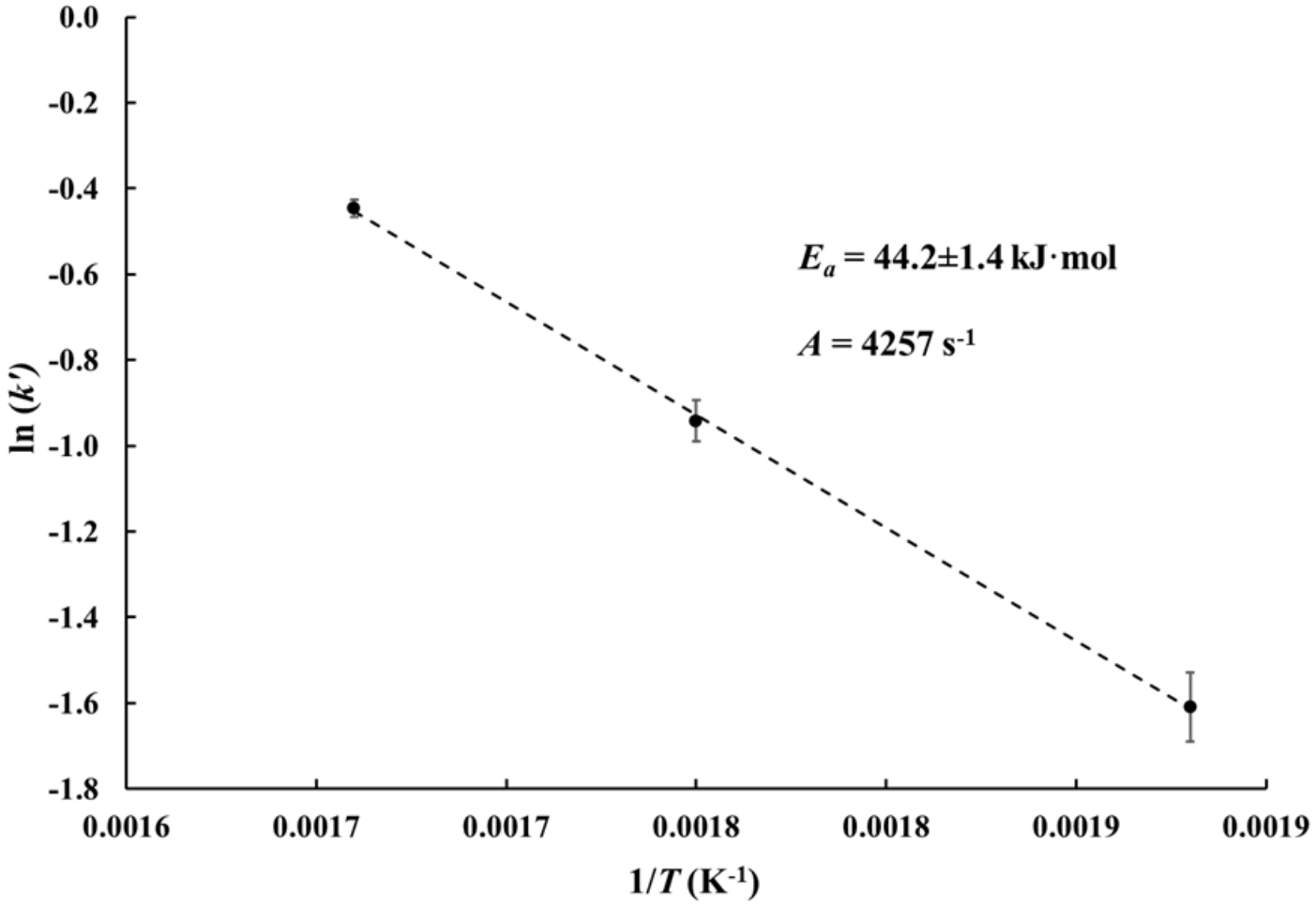

Figure 8. Arrhenius plot for CS_2 conversion across Al_2O_3 under end-of-run conditions using pooled conversion data.

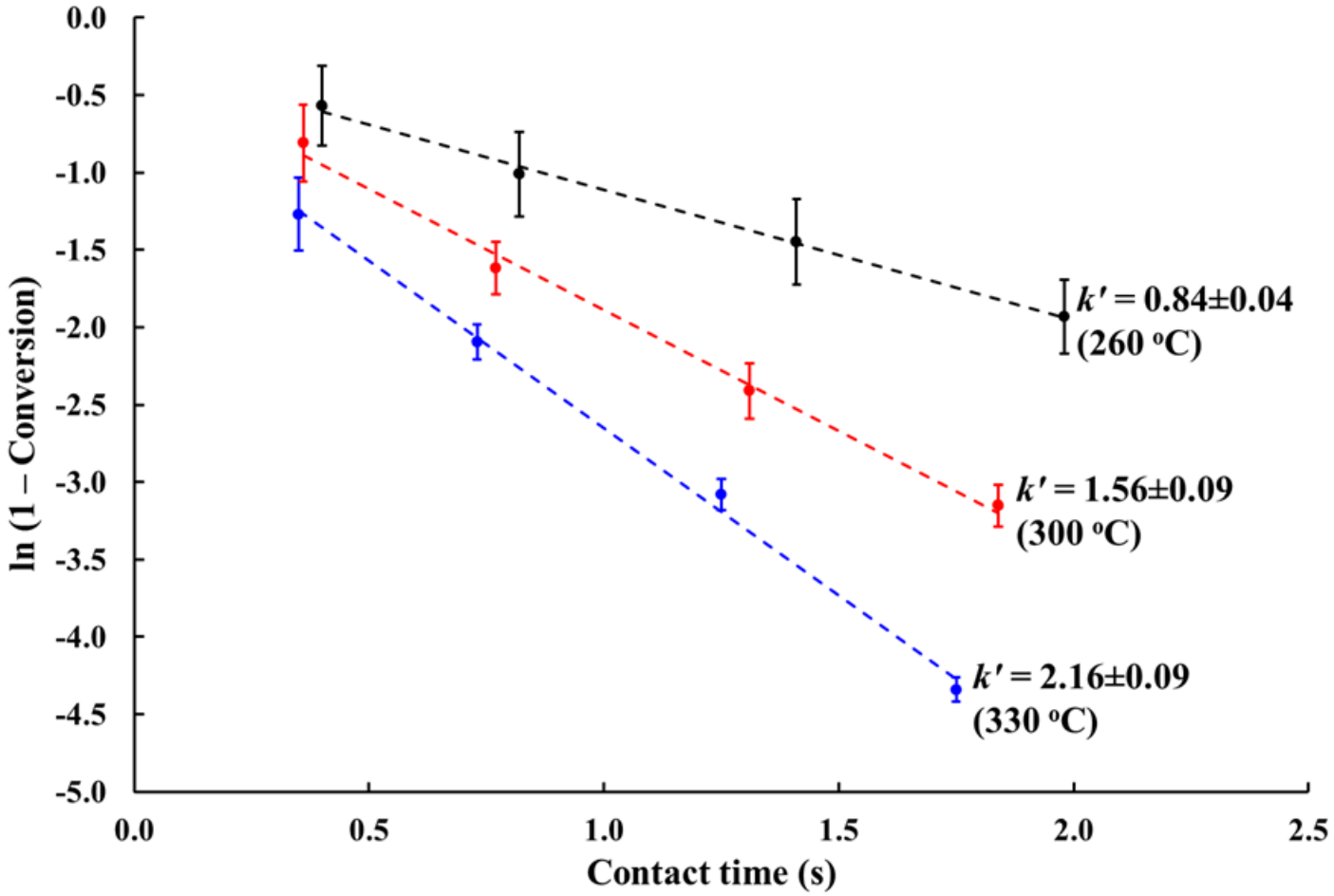

Figure 9. Pseudo-first order plots for COS conversion across Al_2O_3 under end-of-run conditions using pooled conversion data.

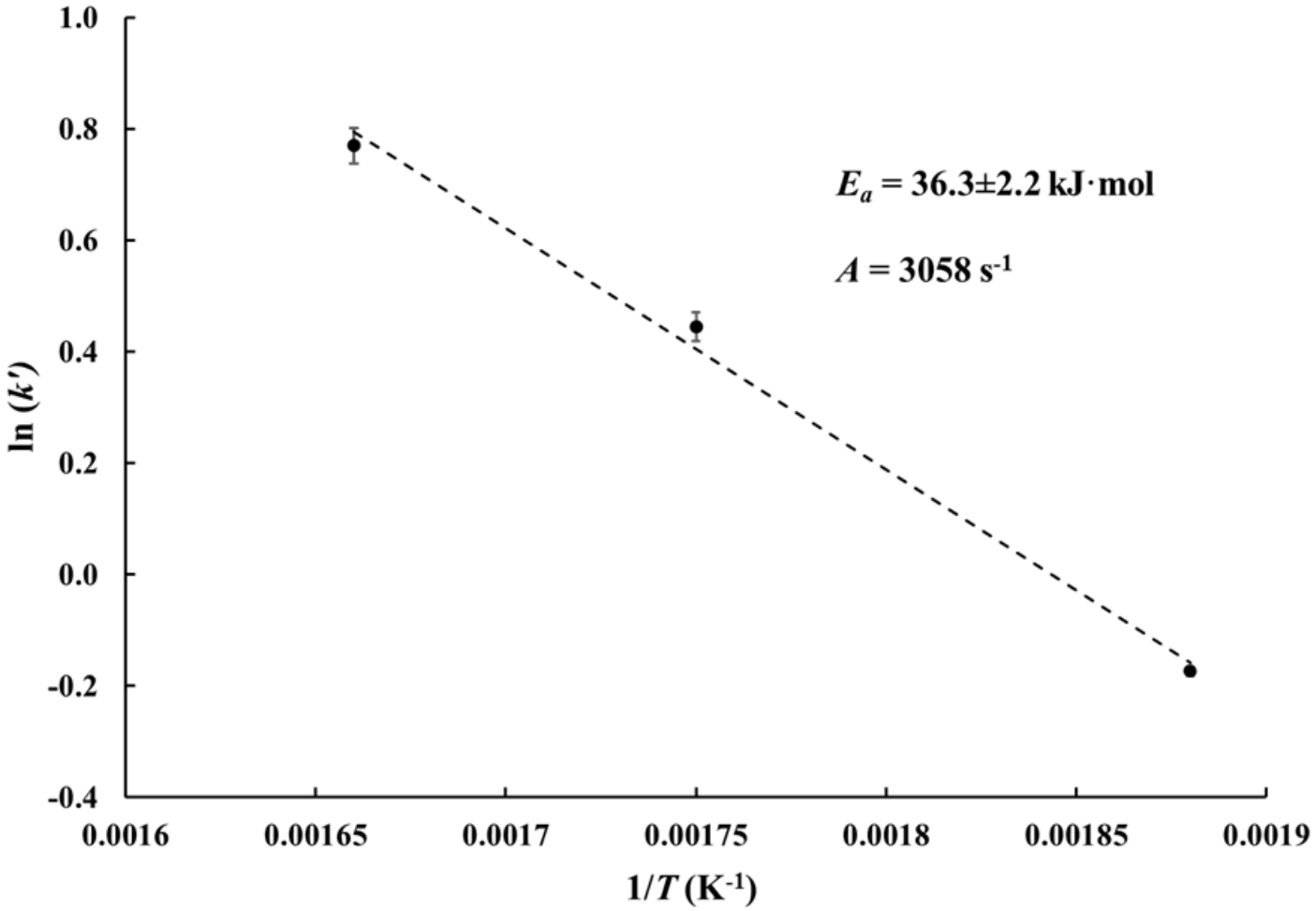

Figure 10. Arrhenius plot for COS conversion across Al_2O_3 under end-of-run conditions using pooled conversion data.

Table 3. Comparison of empirically determined TiO_2 rate constants and kinetic parameters under start-of-run versus end-of-run conditions.

	TiO_2			
	Start-of-run CS_2	**End-of-run CS_2**	**Start-of-run COS**	**End-of-run COS**
260°C / k'	0.46±0.01	0.39±0.01	1.56±0.20	1.32±0.06
300°C / k'	1.45±0.05	0.76±0.02	1.91±0.21	1.97±0.03
330°C / k'	2.48±0.04	1.28±0.06	2.51±0.95	2.59±0.16
E_a (kJ·mol^{-1})	**64.6±5.8**	**45.1±2.0**	**NA**	**25.7±0.2**
A (s^{-1})	**984609**	**10097**	**NA**	**433**

Note that the start-of-run activation energy for CS_2 conversion across Al_2O_3 (Table 2, 57.0±3.7 kJ·mol^{-1}) is lower than that for CS_2 across TiO_2 (Table 3, 64.6±5.8 kJ·mol^{-1}). Additionally, the end-of-run activation energies for CS_2 conversion across Al_2O_3 (Table 2, 44.2±1.4 kJ·mol^{-1}) and TiO_2 (Table 3, 45.1±2.0 kJ·mol^{-1}) are within experimental error of one another. This may seem unexpected at first glance, provided the higher activity of TiO_2 for CS_2 and COS conversion compared to Al_2O_3 under analogous Claus conditions. However, it has been shown that while employing a feed containing just H_2O and CS_2 or H_2O and COS, Al_2O_3 actually outperforms TiO_2 in the corresponding hydrolysis reactions.[14] It is only when the full effects realized under Claus conditions that TiO_2 becomes more active than Al_2O_3. There is good evidence to support that this is related to a higher surface concentration of sulfate species that is established on Al_2O_3 under Claus conditions, which in-turn reduces access to catalyst active sites.[8,13] Indeed, reduction of sulfate by H_2S is more facile on TiO_2 than Al_2O_3 at temperatures employed in Claus catalyst beds.[14] Therefore, the higher CS_2 and COS conversions across TiO_2 can likely be attributed to improved accessibility to catalyst active sites. This would result in a higher turnover frequency that is reflected in the higher pre-exponential factors for TiO_2 (see Tables 2 and 3). The authors are mindful that some surface sulfate is unavoidable under Claus conditions as it is in equilibrium with a necessary thiosulfate intermediate.

The first catalyst bed in the modified Claus process is often a split bed containing both Al_2O_3 and TiO_2 to help maximize CS_2 and COS conversion. While a full bed of TiO_2 would indeed offer higher conversions, cost and susceptibility to fouling from hydrocarbon contamination and / or sooting issues must be considered.[15] Although pure TiO_2 beds are not unheard of, Al_2O_3 is often packed on top of TiO_2 as a "guard" layer when a split bed is employed. In this context, the kinetic parameters reported here can also be applied to a split bed; provided the relative proportions are known and the GHSV for each portion of the bed can be determined.

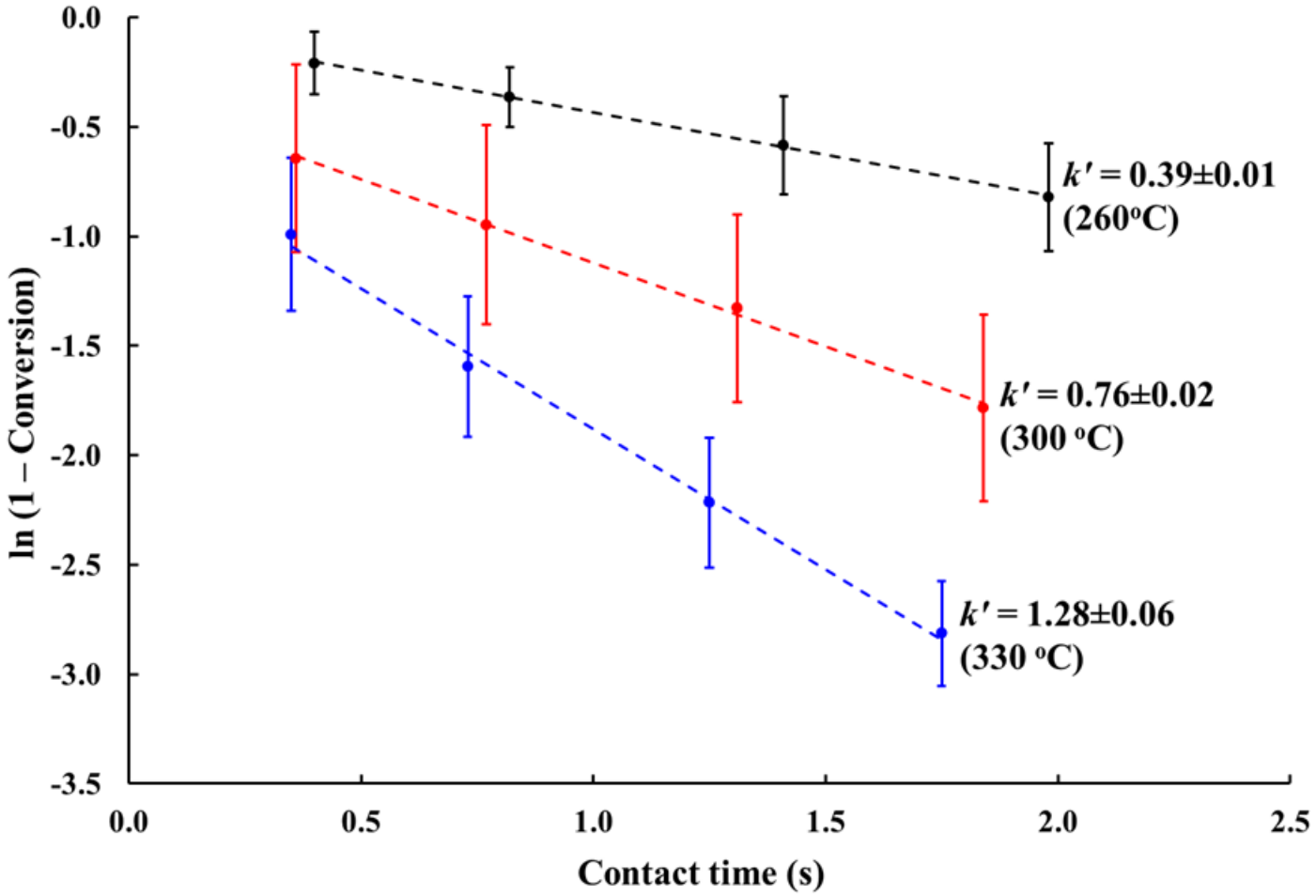

Figure 11. Pseudo-first order plots for CS_2 conversion across TiO_2 under end-of-run conditions using pooled conversion data.

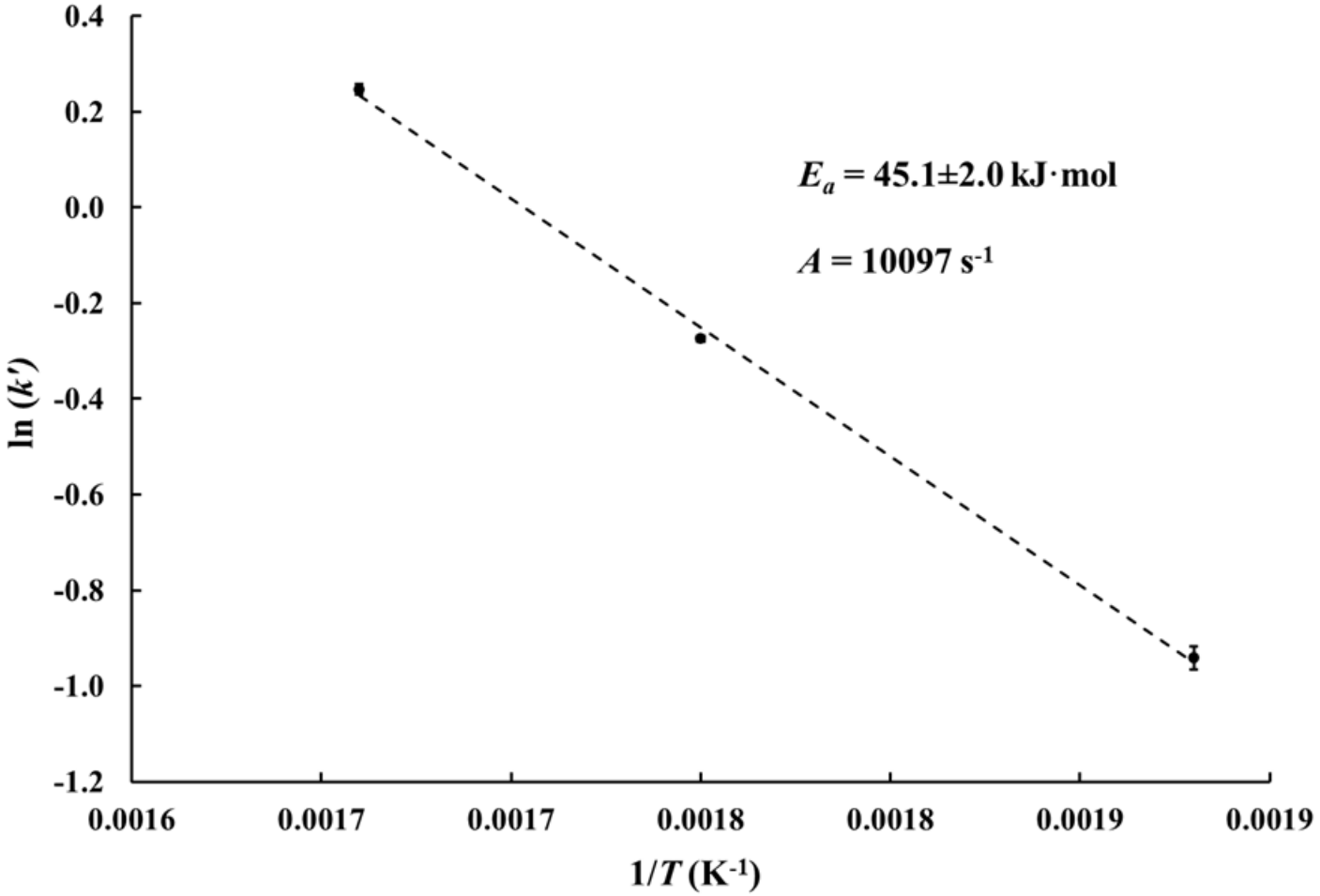

Figure 12. Arrhenius plot for CS_2 conversion across TiO_2 under end-of-run conditions using pooled conversion data.

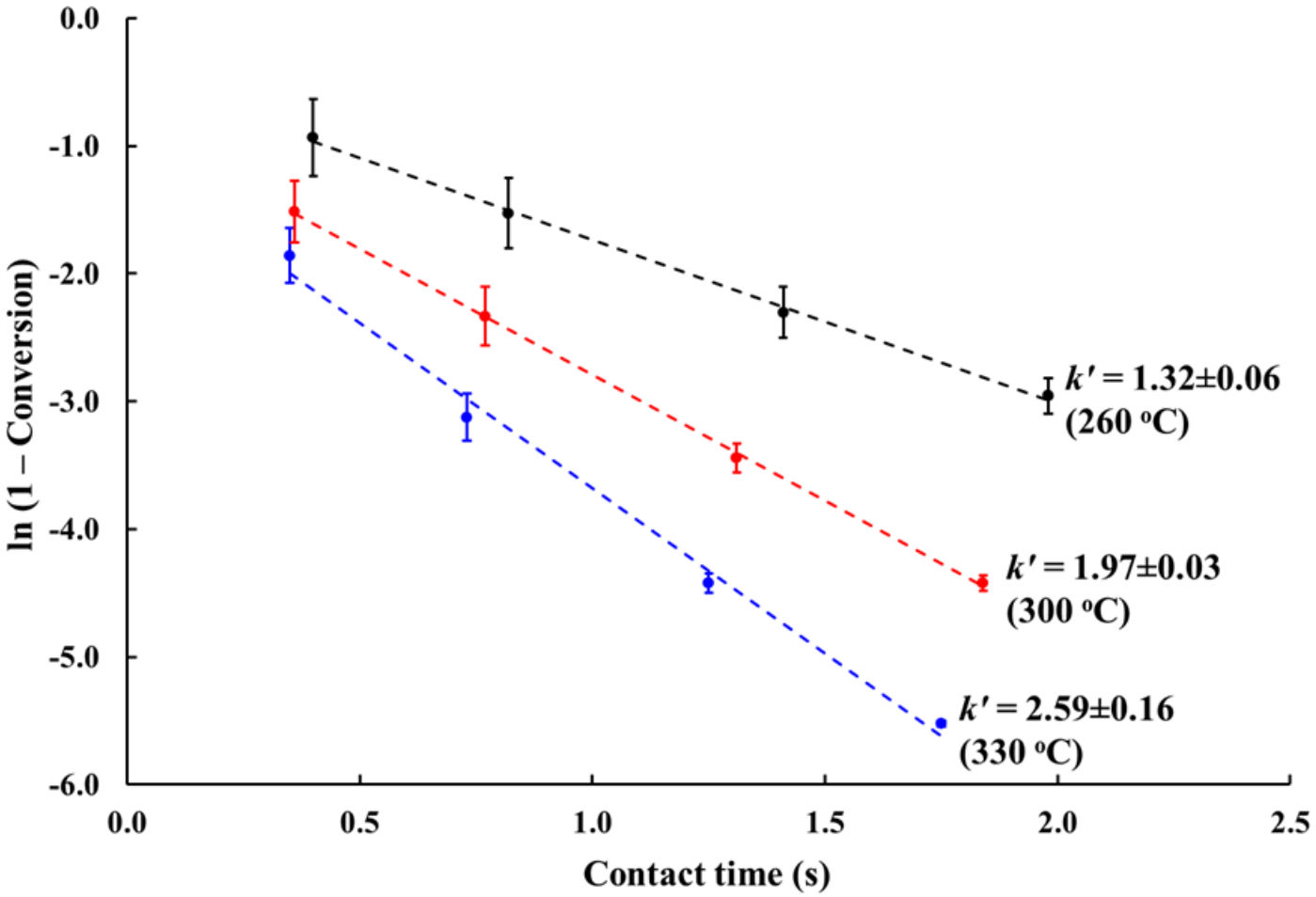

Figure 13. Pseudo-first order plots for COS conversion across TiO_2 under end-of-run conditions using pooled conversion data.

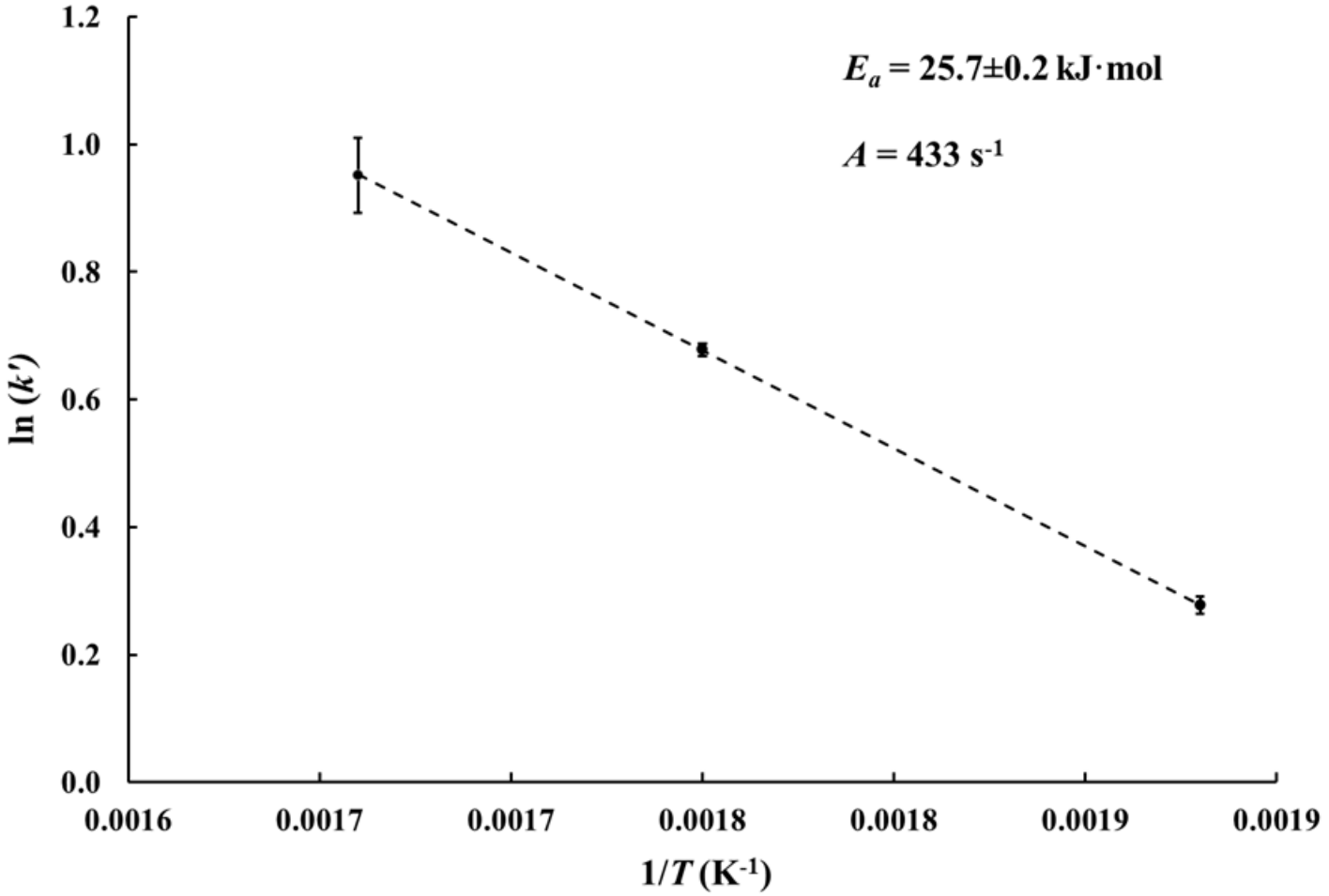

Figure 14. Arrhenius plot for COS conversion across TiO_2 under end-of-run conditions using pooled conversion data.

Conclusions and Future Work

A kinetic study was performed on several commercial high-performance Claus Al_2O_3 and TiO_2 catalysts under end-of-run conditions and the results were compared to those from our previously published start-of-run kinetic study. Except for the COS reaction across Al_2O_3, the average end-of-run conversions were generally lower than the start-of-run conversions and this was reflected in the obtained rate constants and kinetic parameters. There was generally more variation in performance between the different Al_2O_3 samples compared to the various TiO_2 materials that were tested. However, these differences in performance were most evident under the more stringent test conditions. At the lower and more typical GHSVs that would be applied in the field, the differences in performance were less noticeable. Finally, as mentioned above, the Al_2O_3 samples employed in this study were high-performance activated materials. As such, the kinetic parameters determined here will likely afford conservative approximations for promoted Al_2O_3 materials.

References

1. Website: http://www.essentialchemicalindustry.org/chemicals/sulfuric-acid.html (accessed November 2021).
2. U.S. Geological Survey. Mineral Commodity Summaries, 2019.
3. Clark PD, Dowling NI, Huang M, Svrcek WY. Mechanisms of CO and COS Formation in the Claus Furnace, Ind. Eng. Chem. Res., 2001; 40, 497-508.
4. Ray JL and Nedez C. New Concepts for a New Generation Claus Alumina, Catal Today, 1996; 29, 139-142.
5. Tong S, Dalla Lana IG and Chuang KT. Kinetic Modelling of the Hydrolysis of Carbonyl Sulfide Catalyzed by Either Titania or Alumina, Can J Chem Eng, 1993; 71, 392-400.
6. Tong S, Dalla Lana IG and Chuang KT. Kinetic Modelling of the Hydrolysis of Carbon Disulfide Catalyzed by Either Titania or Alumina, Can J Chem Eng, 1995; 73, 220-228.
7. Clark PD, Dowling NI and Huang M. How Do Claus Catalysts Really Work? The 52nd Laurance Reid Gas Conditioning Conference, Norman, Oklahoma, USA, February 24-27, 2002.
8. Lavery CB, Dowling NI and Clark PD. Examining the Effect of H_2S:SO_2 Ratios on CS_2 Conversion at First Catalytic Convert Conditions, Alberta Sulphur Research Quarterly Bulletin, 2015; 52, 45.
9. Lavery CB, Sui R, Lotfali M and Marriott RA. Kinetic Studies for the Hydrolysis of CS_2 and COS Across the Claus Catalytic Converters. Brimstone Sulfur Recovery Symposium, Vail, Colorado, USA, September 16-20, 2019.
10. Lavery CB, Sui R, Deering CE, Lesage KL and Marriott RA. Upgrades to ASRL Bench Scale Catalyst Testing System, Alberta Sulphur Research Quarterly Bulletin, 2015; 52, 45
11. Clark PD, Dowling NI and Huang M. Titania as a Claus Catalyst, Alberta Sulphur Research Quarterly Bulletin, 2020; No. 195, Vol. LVIII.
12. Clark PD, Dowling NI and Huang M. Conversion CS2 and COS over Alumina and Titania under Claus Process Conditions: Reaction with H_2O and SO_2, Appl Catal B, 2001; 31, 107-112.
13. Kijlstra WS, Clark PD and Huang M. Putting Claus Catalysts to the Test, Sulphur; 2001; 276, 71-79.
14. Laperdrix E, Justin I, Costentin G, Saur O, Lavalley JC, Aboulayt A, Ray JL and Nedez C. Comparative Study for CS_2 Hydrolysis Catalyzed by Alumina and Titania, Appl Catal B, 1998; 17, 167-173.
15. Lavery CB, Marrugo-Hernandez JJ, Sui R, Dowling NI and Marriott RA. The Effect of Methanol in the First Catalytic Converter of the Claus Sulfur Recovery Unit, Fuel, 2019; 238, 385-393.